Substantially enhanced high-temperature capacitive performance in BOPP films via coating with a magnetic inorganic nanolayer

Hai Sun[a, b, 1], Shuang Liang[a, b, 1], Zhaoliang Xing[c, d, 1], Shengkun Niu[a, b], Chao Yin[a, b], Yue Zhang[a, b], Changhai Zhang[a, b], Lin Li[e], Tiandong Zhang[a, b, *], Qingguo Chi[a, b]

a Key Laboratory of Engineering Dielectrics and Its Application, Ministry of Education, Harbin University of Science and Technology, Harbin, China
b School of Electrical and Electronic Engineering, Harbin University of Science and Technology, Harbin, China
c State Key Laboratory of Alternate Electrical Power System with Renewable Energy Sources, North China Electric Power University, Beijing, China
d China Electric Power Research Institute Company Limited, Beijing, China
e Electric Power Research Institute of State Grid Heilongjiang Electric Power Co., Ltd., Harbin, China

[1]Co-first authors: Hai Sun, Shuang Liang, Zhaoliang Xing
*Corresponding author: tdzhang@hrbust.edu.cn (Tiandong Zhang)

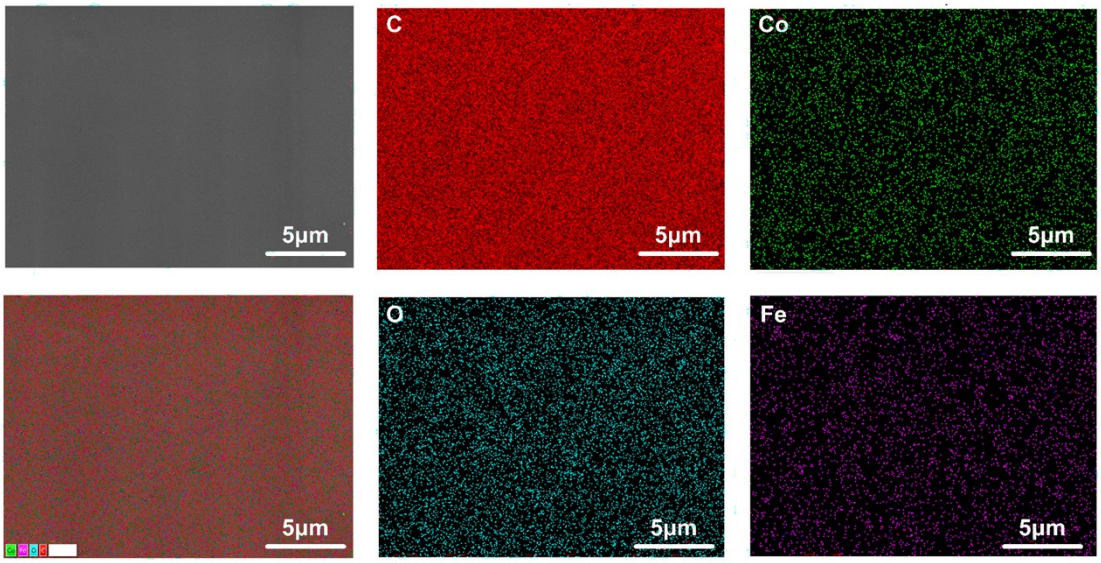

Fig. S1 Surface morphology and characteristic element distribution of CoFe2O4/BOPP/CoFe2O4 composite film.

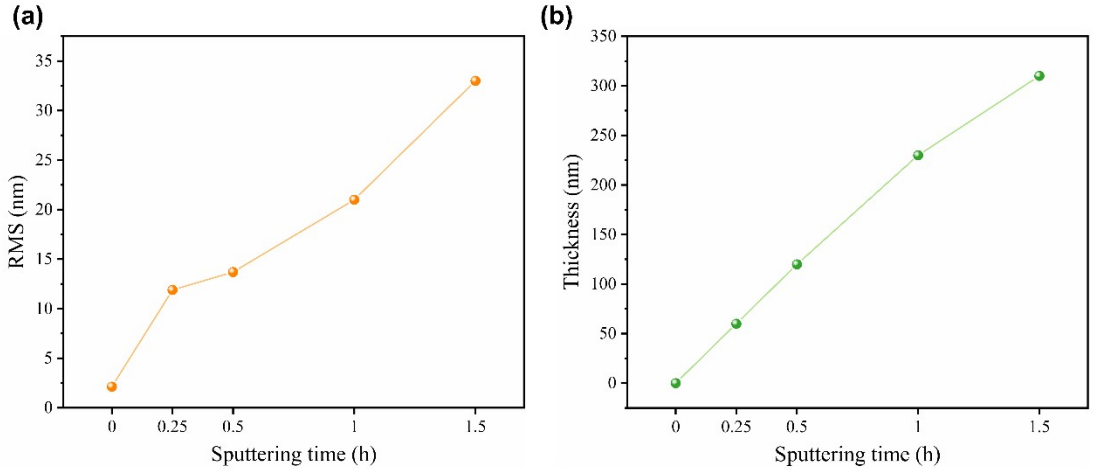

Fig. S2 (a) A variation in thickness was observed at different sputtering times. (b) Root-mean-square (RMS) of the $CoFe_2O_3$ coating layer versus sputtering time.

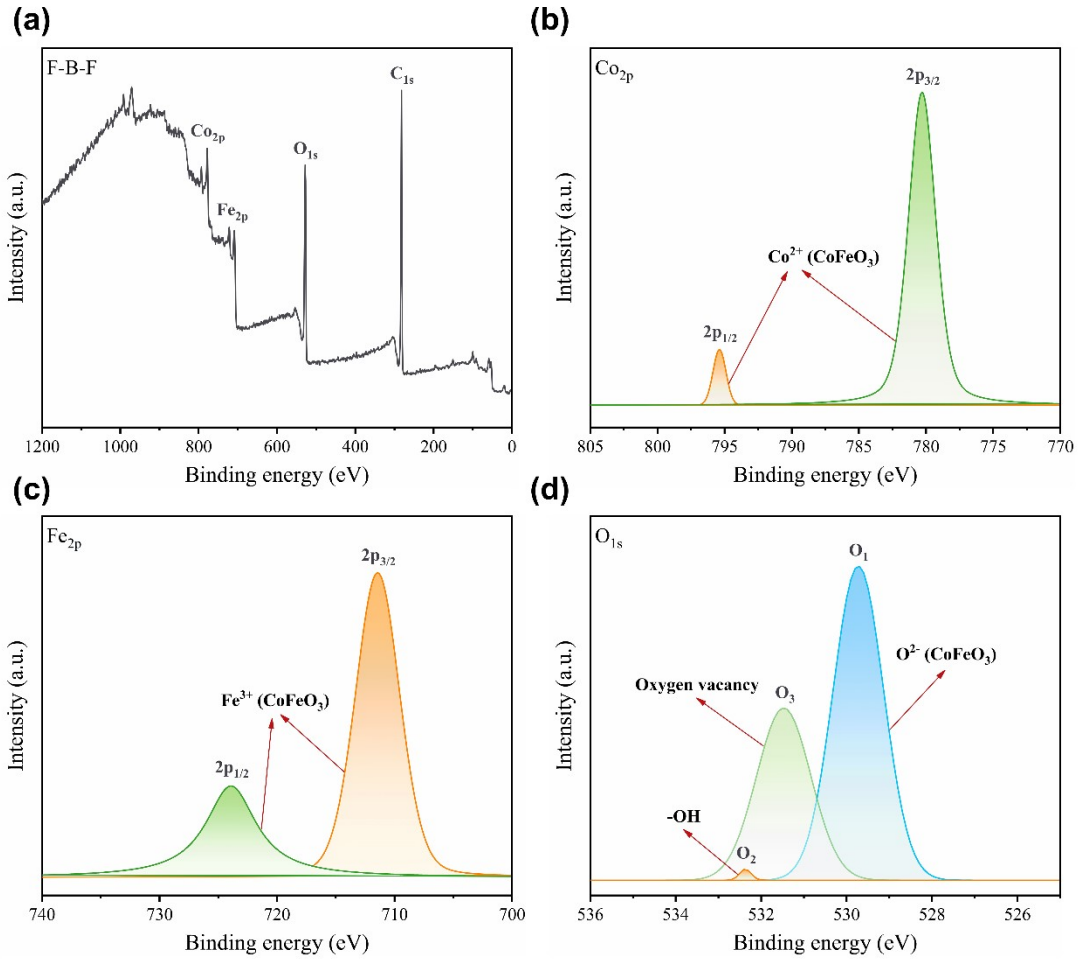

Fig. S3 (a) XPS spectra of BOPP films coated with varying thicknesses of inorganic nanolayers. (b) XPS spectra for the Co_{2p} peak. (c) XPS spectra for the Fe_{2p} peak. (d) XPS spectra for the O_{1s} peak. As demonstrated, the characteristic peaks at 795.4 eV vs. 779.9 eV confirm the presence of Co^{2+}, 710.3 eV vs. 723.9 eV confirm the presence of Fe^{3+}, and 529.9 eV show typical chemical oxygen-metal bond, which matched with the spinel structure. Furthermore, the residual air in the deposition chamber led to the composite exhibiting characteristic peaks indicated the vacancies of highly oxidative oxygen (531.8 eV), and the peak at 533.23 eV was ascribed to the OH^- about the surface-adsorbed oxygen groups.

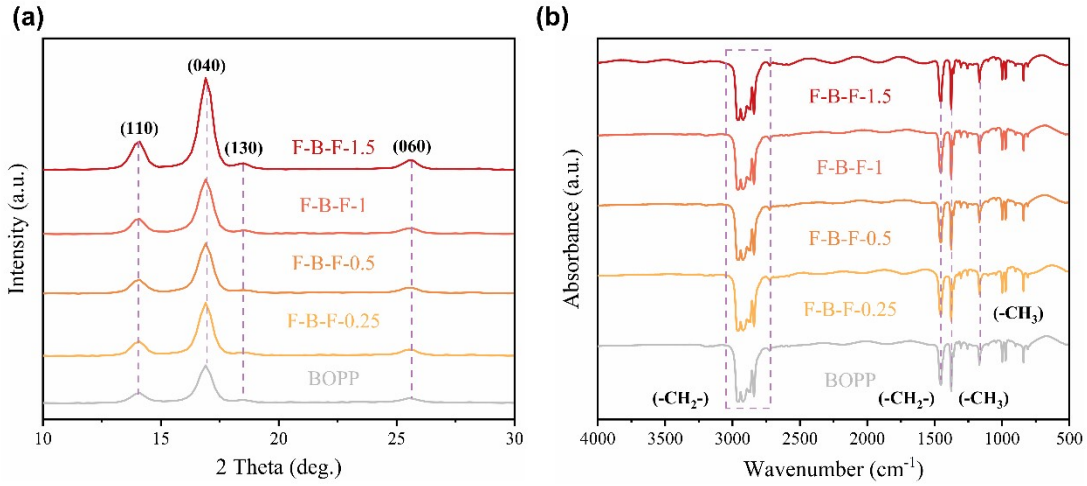

Fig. S4 The microstructure of BOPP films coated with varying thicknesses of inorganic nanolayers. (a) XRD spectra. (b) FTIR spectra.

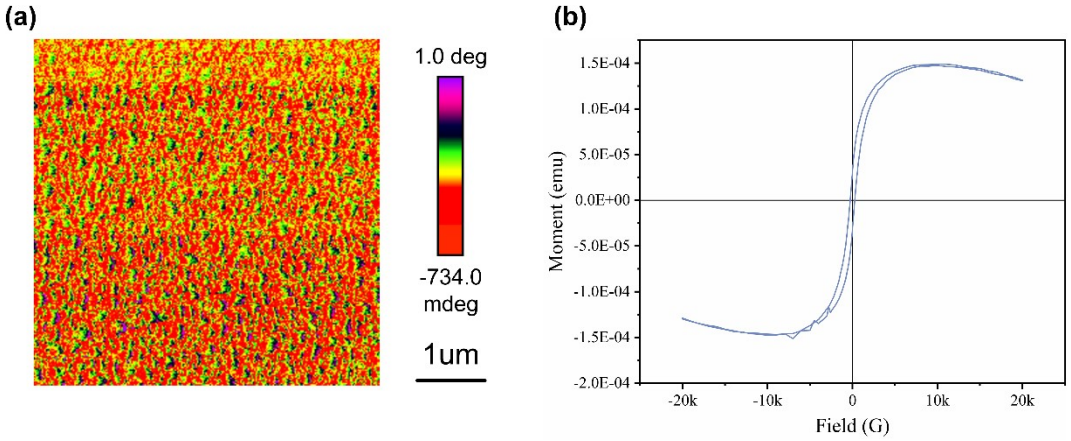

Fig. S5 (a) The magnetic domain morphology of $CoFe_2O_3$ was observed using magnetic force microscope (MFM). In the context of MFM, chromatic aberration is defined as the degree of bias between the magnetization vector and the magnetic probe. (b) The magnetic hysteresis loop of $CoFe_2O_3$.

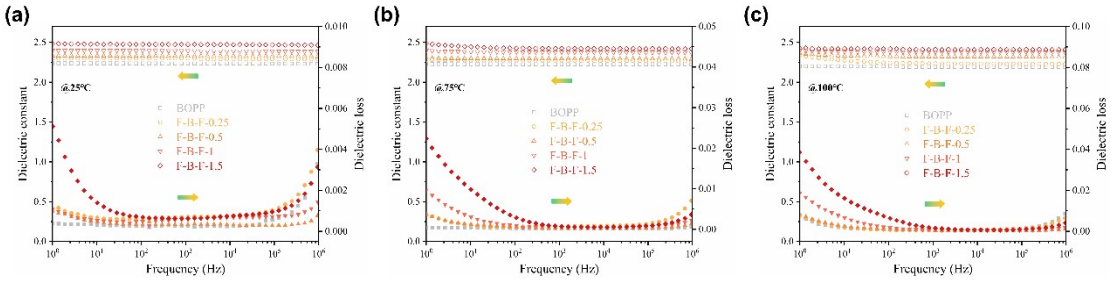

Fig. S6 The frequency dependence of permittivity and dielectric loss of BOPP films coated with varying thicknesses of inorganic nanolayers. (a) at 25℃. (b) at 75℃. (c) at 100℃.

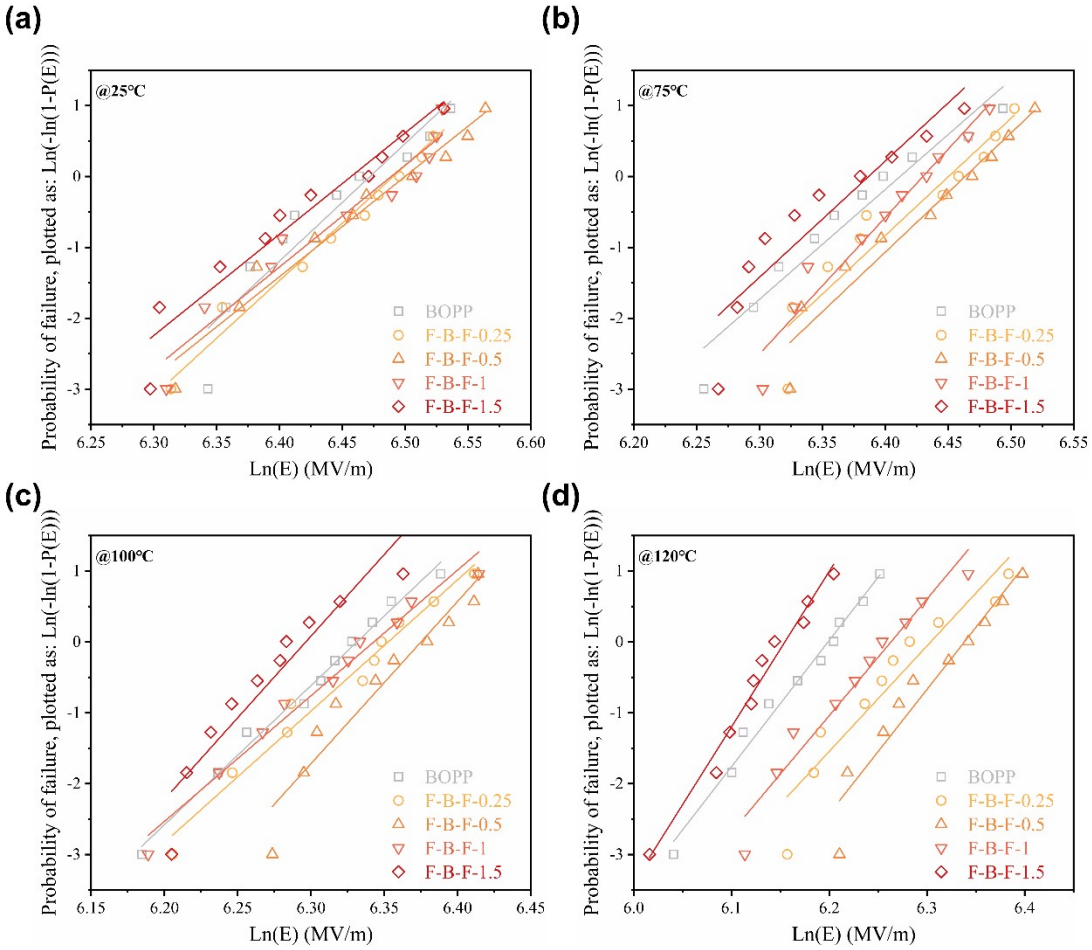

Fig. S7 The Weibull breakdown strength of BOPP films coated with varying thicknesses of inorganic nanolayers. (a) at 25℃. (b) at 75℃. (c) at 100℃. (d) at 120℃.

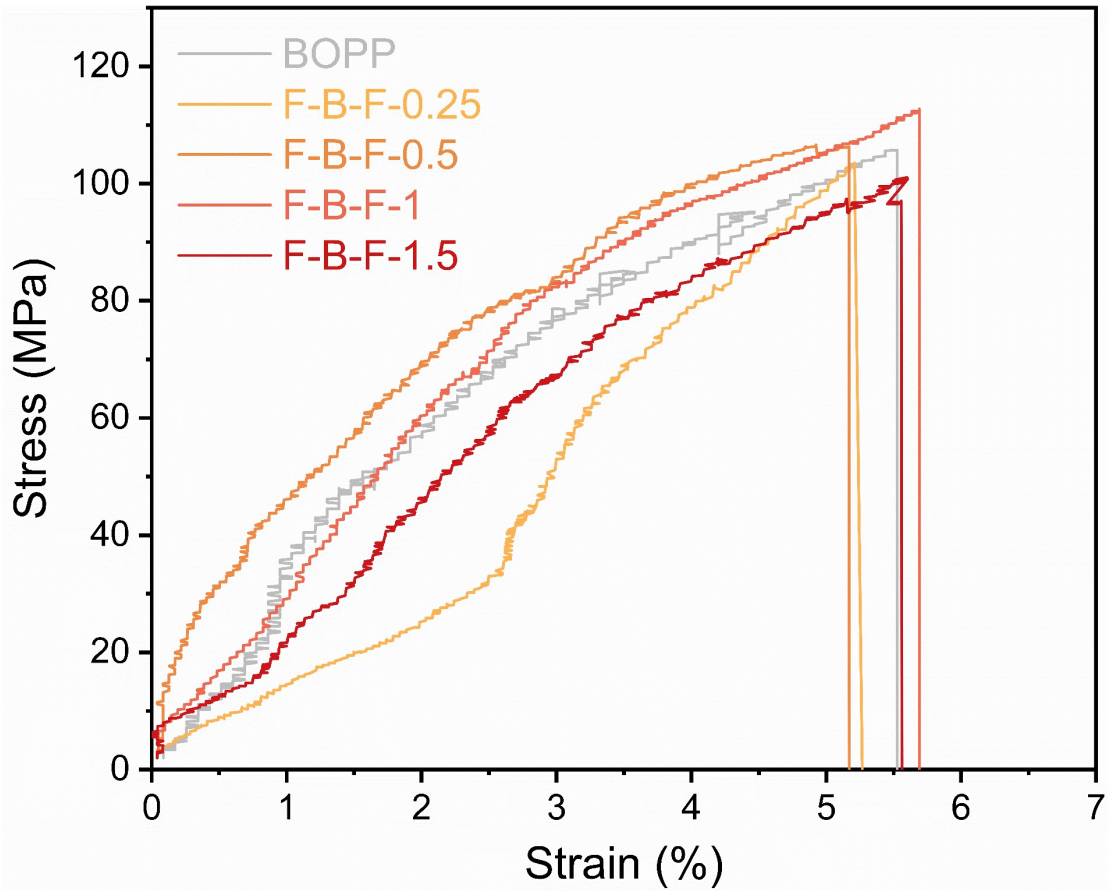

Fig. S8 Stress-strain curves of BOPP film and composite films with varying thicknesses of inorganic nanolayers.

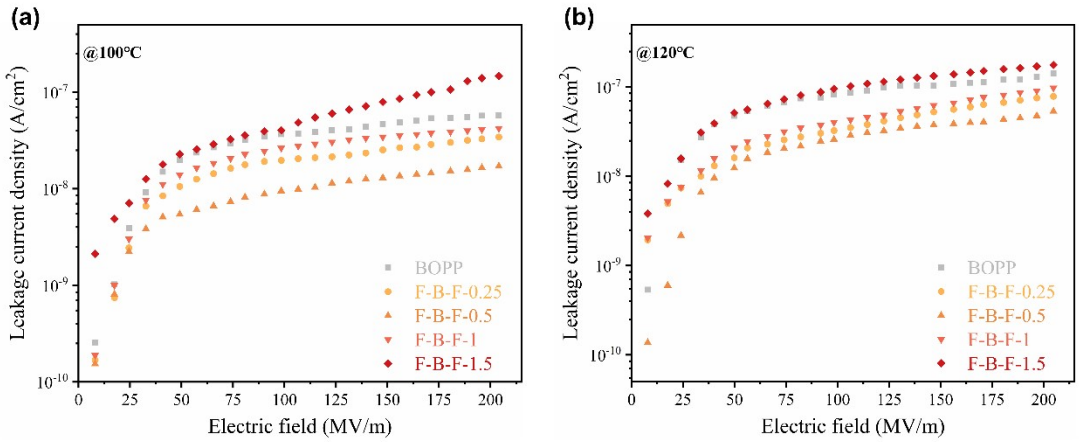

Fig. S9 The leakage current density of BOPP films coated with varying thicknesses of inorganic nanolayers. (a) at 100℃. (b) at 120℃.

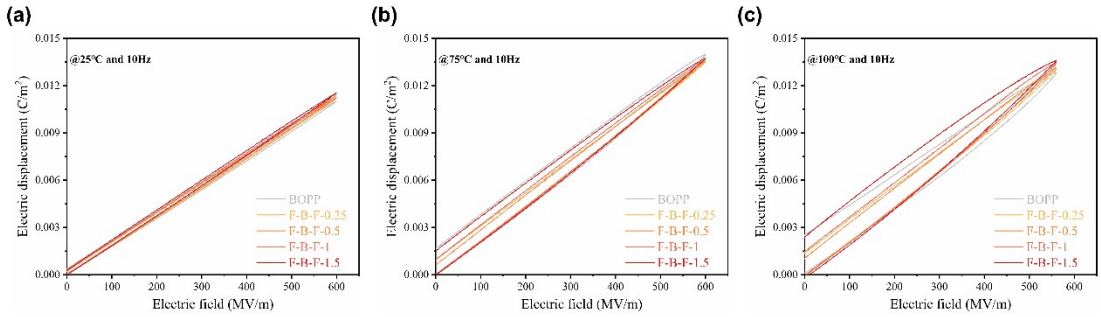

Fig. S10 The D-E loops of BOPP films coated with varying thicknesses of inorganic nanolayers. (a) at 25℃ and 600 MV/m. (b) at 75℃ and 600 MV/m. (c) at 100℃ and 560 MV/m.

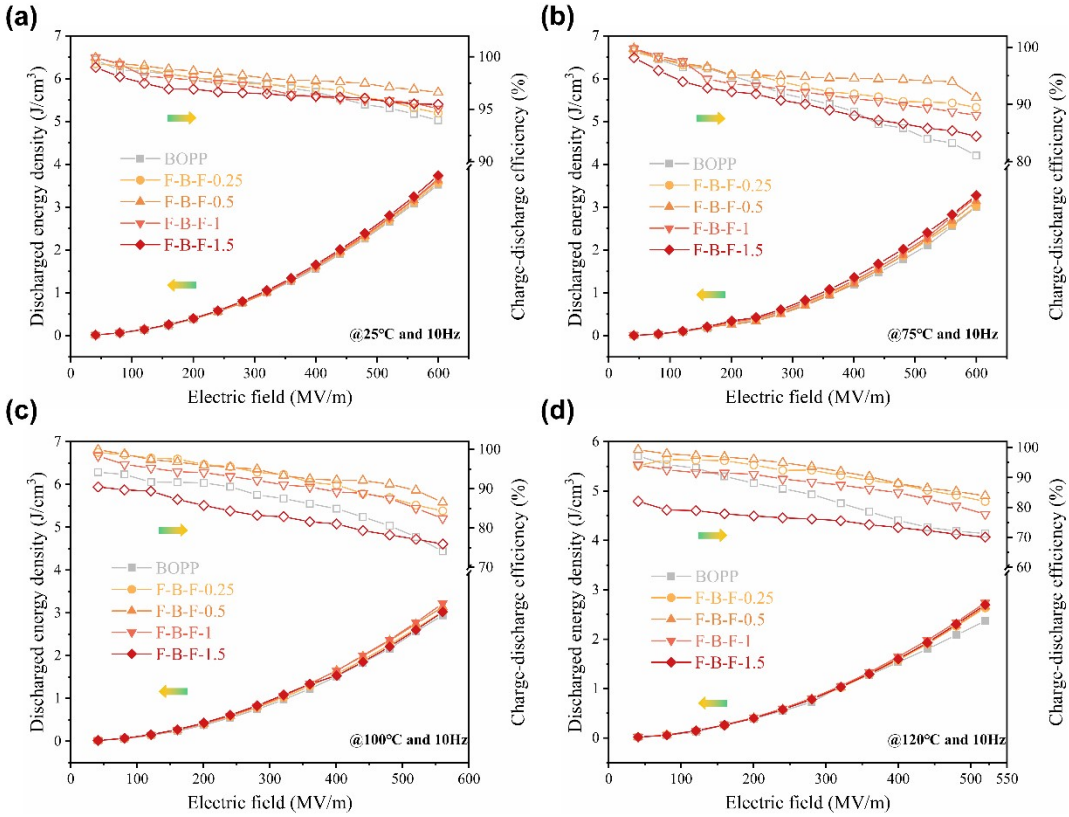

Fig. S11 The energy storage performance of BOPP films coated with varying thicknesses of inorganic nanolayers. (a) at 25℃. (b) at 75℃. (c) at 100℃. (d) at 120℃.

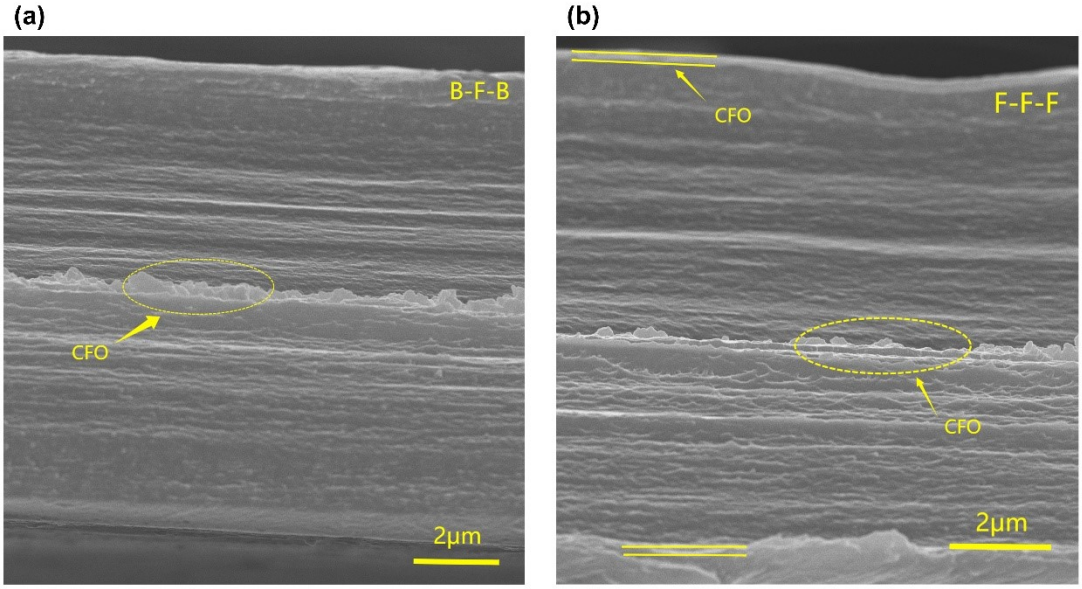

Fig. S12 Cross-sectional SEM images of BOPP films coated with inorganic coating nanolayers at varying locations. (a) B-F-B composite film. (b) F-F-F composite film.

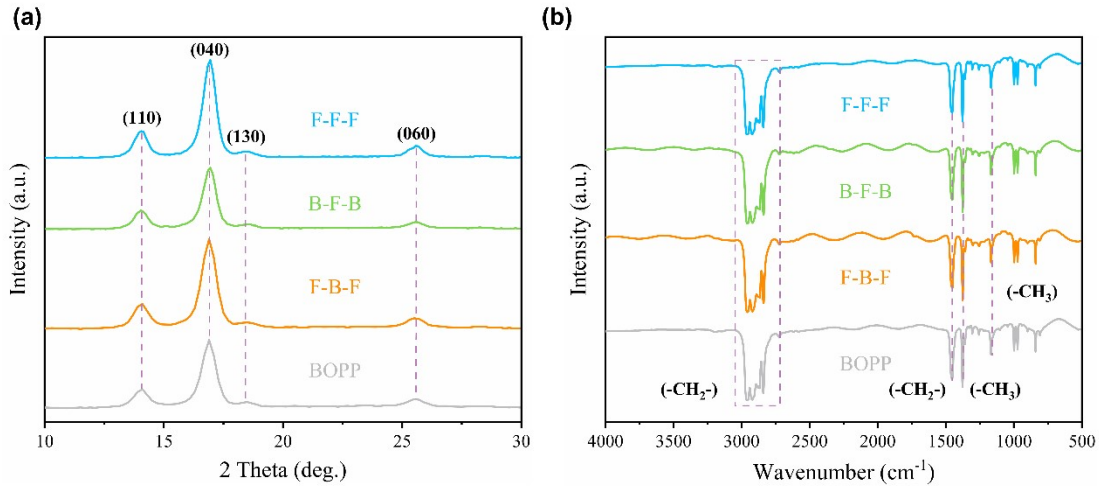

Fig. S13 The microstructure of BOPP films coated with inorganic coating nanolayers at varying locations. (a) XRD spectra. (b) FTIR spectra.

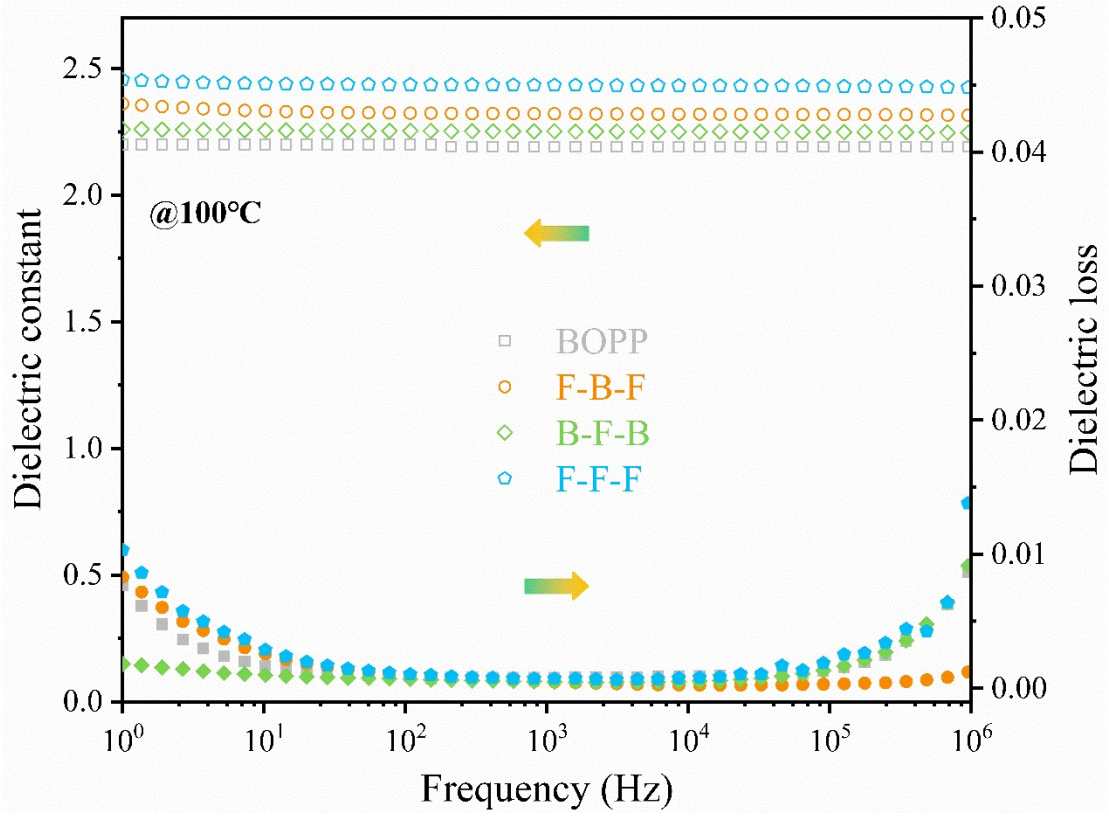

Fig. S14 The frequency dependence of permittivity and dielectric loss of BOPP films coated with inorganic coating nanolayers at varying locations at 100°C.

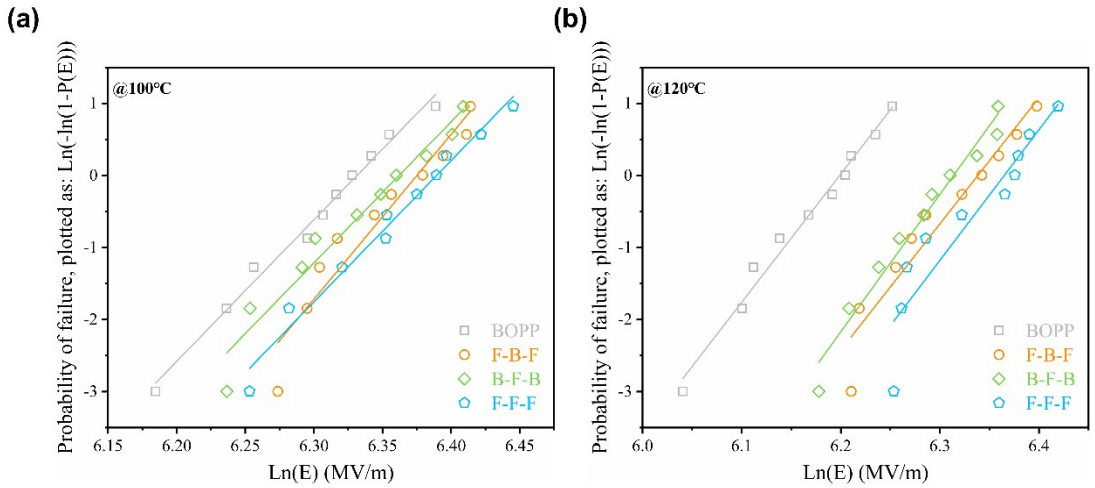

Fig. S15 The Weibull breakdown strength of BOPP films coated with inorganic coating nanolayers at varying locations. (a) at 100°C. (b) at 120°C.

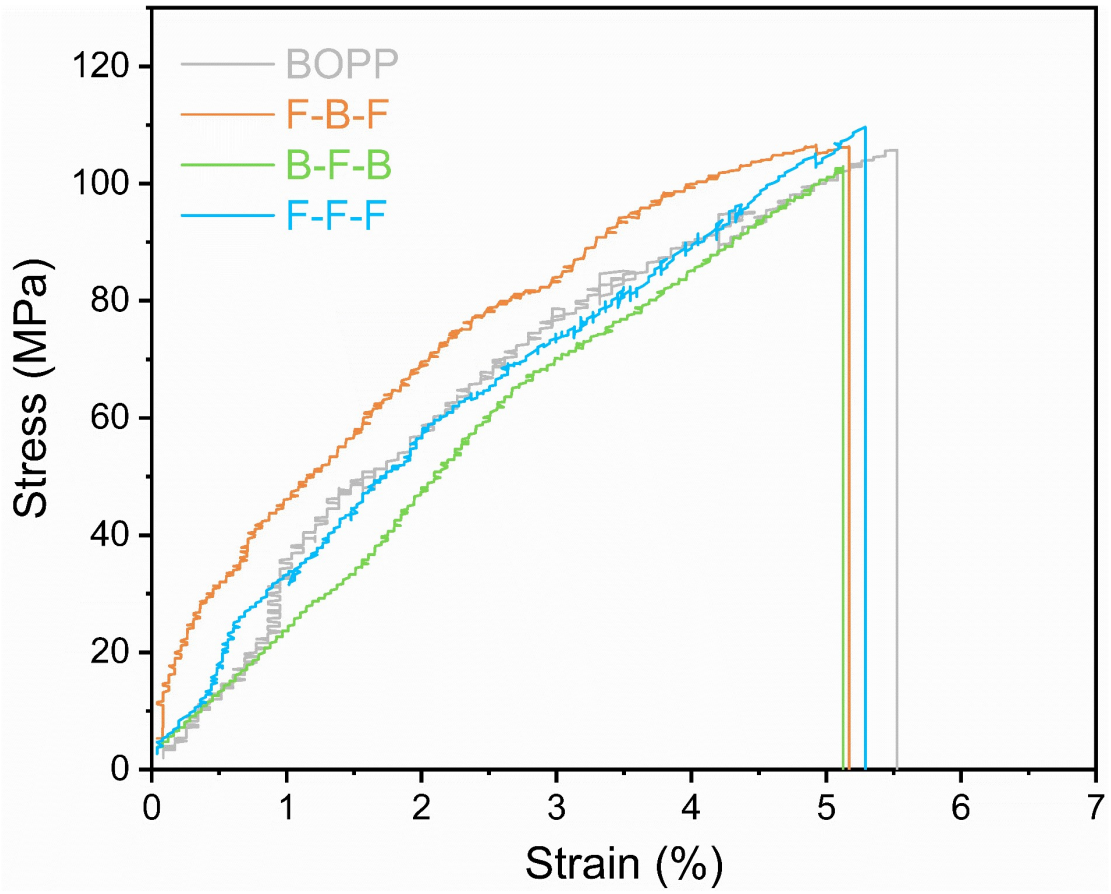

Fig. S16 Stress-strain curves of BOPP film and composite films with different structures.

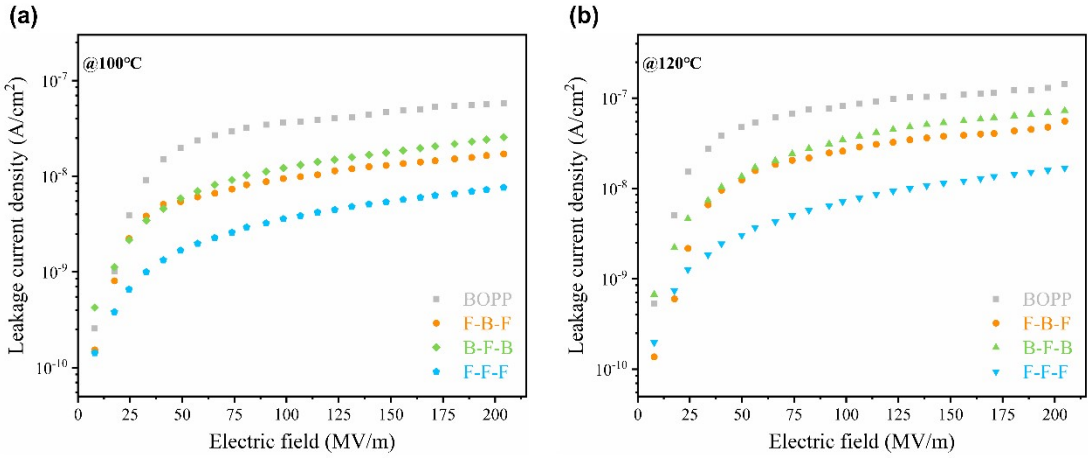

Fig. S17 The leakage current density of BOPP films coated with inorganic coating nanolayers at varying locations. (a) at 100℃. (b) at 120℃.

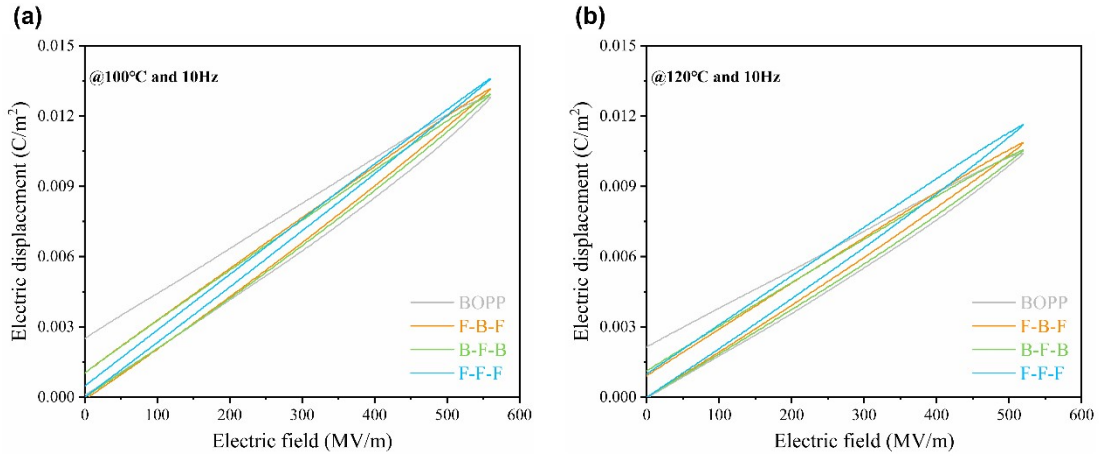

Fig. S18 The D-E loops of BOPP films coated with inorganic coating nanolayers at varying locations. (a) at 100℃ and 560 MV/m. (b) at 120℃ and 520 MV/m.

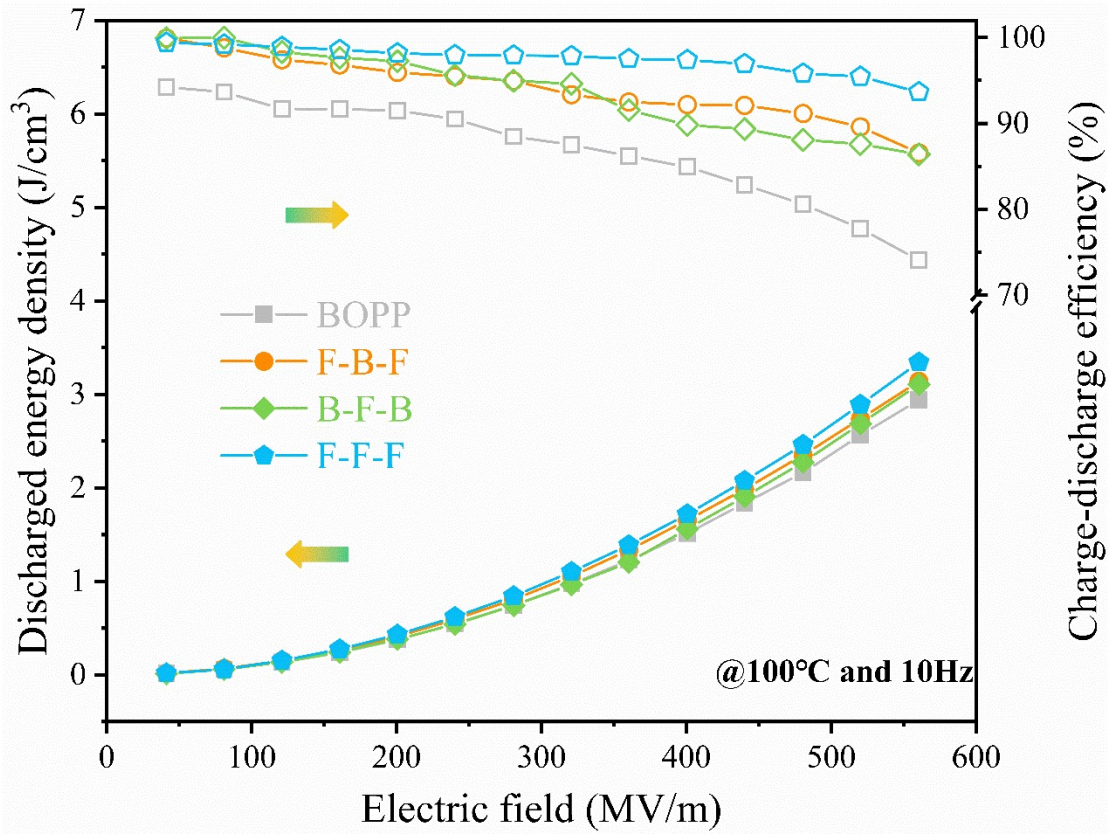

Fig. S19 The energy storage performance of BOPP films coated with inorganic coating nanolayers at varying locations at 100℃.